Magneto-optical study of anomalous magnetization reversal in the presence of anisotropy dispersion in CoPd thin films

Mehran Sedrpooshan and Hossein Ahmadvand*
Department of Physics, Isfahan University of Technology, Isfahan 84156-83111, Iran

Diego López González and Sebastiaan van Dijken
NanoSpin, Department of Applied Physics, Aalto University School of Science, P.O. Box 15100, FI-00076 Aalto, Finland

(Received 19 July 2018; revised manuscript received 8 November 2018; published 28 December 2018)

Magnetization reversal is investigated in the presence of anisotropy dispersion in weakly disordered Co_xPd_{100-x} ($x = 23, 36, 43$) thin films. A fourfold in-plane magnetic anisotropy is observed for $x = 23$, whereas an increase of the Co:Pd ratio induces a uniaxial anisotropy in $x = 36$ and 43 films. Anomalous magnetization reversal appears along the hard axes (referred to as collapse of hard axes) in $x = 23$ and 36 films, but disappears for $x = 43$. The results are consistent with the two-grain Stoner-Wohlfarth model. It is argued that the collapse of the hard axes can be controlled by intergranular exchange interaction. Quadratic magneto-optical Kerr effect (QMOKE) is also observed in the films and is found to weaken if the in-plane anisotropy is lowered through the Co:Pd ratio. QMOKE is observed for magnetic field orientations near the hard axes but not exactly along it, in agreement with the two-grain Stoner-Wohlfarth model.

DOI: 10.1103/PhysRevB.98.214444

I. INTRODUCTION

Studies on magnetic thin films are mainly driven by their key role in spintronics, sensors, microelectromechanical systems, and magnetic data storage devices. An accurate recognition of magnetic properties in this two dimensional geometry is required for different applications. In this regard, magnetization reversal data give a lot of information about magnetic anisotropy [1,2], exchange bias coupling [3,4], exchange spring effect [5–7], etc. Magnetization reversal is particularly complex in magnetic systems with large anisotropy dispersion, as highlighted by numerous studies [8–13].

Magnetic anisotropy is one of the most important parameters of magnetic thin films in practical applications [14–16]. Among magnetic materials, binary alloys of transition metals including FePt, FePd, CoPt, and CoPd have attracted enormous interest mostly because of their high magnetocrystalline anisotropy energy [17–19].

Pd is a paramagnetic metal which is near the Stoner criterion limit for becoming a spontaneous ferromagnet. According to electron band structure calculations, 1.5 percentage of Co can induce ferromagnetic ordering in CoPd [20]. In such Pd rich alloys, Co moments polarize the itinerant electrons of Pd. However, a limited number of Pd atoms are affected by Co magnetic moments and an increase of magnetism requires larger Co:Pd ratios. Because of this large tunability, the CoPd alloy has manifested itself as a model system for investigations on exchange interaction, spin-orbit coupling, and magnetization reversal, which are of great importance for fundamental studies and applications.

CoPd thin films and multilayers have received interest because of perpendicular magnetic anisotropy [21], the observation of stable Néel skyrmions [22], applications in perpendicular magnetic tunnel junctions [23], hydrogen gas sensing, and other spintronic devices [24–29]. Despite many works on CoPd thin films, details on the in-plane anisotropy and its dependence on the Co:Pd ratio have not been reported. In the present study, it is shown that the Co:Pd ratio greatly influences the in-plane anisotropy and anisotropy dispersion. Furthermore, the impact of intergranular exchange interaction on magnetization reversal is investigated in the presence of anisotropy dispersion. Our results demonstrate a collapse of the magnetic hard axis in films with small Co:Pd ratios. This effect is eliminated by an enhancement of intergranular exchange interaction in films with larger Co:Pd ratios. We show that our results are well described by the two-grain Stoner-Wohlfarth model. In addition, QMOKE is observed in films with strong magnetic in-plane anisotropy (i.e., small Co:Pd ratios). As an auxiliary method, QMOKE confirms the validity of the two-grain Stoner-Wohlfarth model for the interpretation of our magnetization reversal data on weakly disordered CoPd thin films.

II. EXPERIMENT

The preparation of CoPd thin films by pulsed laser deposition (PLD) is uncommon and rarely reported [30]. In this study, we used this method to deposit Co_xPd_{100-x} thin films with three different compositions of $x = 23$, 36, and 43 on single crystalline MgO (001) substrates. For this purpose, a KrF excimer laser (Lambda Physik) with a wavelength of 248 nm, pulse duration of 20 ns, energy per pulse of 200 mJ, and repetition rate of 6 Hz was used. A low growth rate of 1.2 nm/min was obtained, which resulted in a homogeneous

*ahmadvand@cc.iut.ac.ir.

TABLE I. Structural parameters of CoPd thin films obtained from XRR and XRD patterns.

Sample	Diffusion layer thickness (nm)	Main layer thickness (nm)	Total thickness (nm)	Main layer density (gr/cm^3)	Lattice constant (Å)
$Co_{23}Pd_{77}$/MgO	1.1 ± 0.1	17.3 ± 0.1	18.4 ± 0.1	10.47	3.82
$Co_{36}Pd_{64}$/MgO	0.8 ± 0.1	14.5 ± 0.2	15.3 ± 0.2	10.38	3.79
$Co_{43}Pd_{57}$/MgO	0.6 ± 0.1	14.8 ± 0.3	15.4 ± 0.3	10.14	3.77
$Co_{23}Pd_{77}$/MgO	1.5 ± 0.2	36.3 ± 0.3	37.8 ± 0.3	10.31	3.80

CoPd alloy. The target was composed of separate high purity metallic Pd and Co disks that were periodically exposed to the laser beam by continuous rotation. The films were deposited at room temperature in a base pressure below 2×10^{-6} Torr and then annealed *in situ* at 400 °C for 10 min in high vacuum. The short heat treatment resulted in partial epitaxy with considerable anisotropy dispersion in the films. For comparison, a film was also directly deposited at a substrate temperature of 400 °C.

The composition of the CoPd films were measured by energy-dispersive x-ray spectroscopy (EDS) using a FEI Quanta 200 ESEM and SEM micrographs were obtained by using a Hitachi S-4800 scanning electron microscope. X-ray diffraction (XRD) and x-ray reflectivity (XRR) patterns were obtained by a Rigaku SmartLab diffractometer. Magnetic hysteresis loops of the films were measured using magneto-optical Kerr effect (MOKE) by a Kerr microscope (Evico magnetics GmbH). Ferromagnetic resonance was investigated using a vector network analyzer (VNA-FMR) in the presence of a 100 mT magnetic bias field at room temperature.

III. RESULTS AND DISCUSSION

A. Structural features

Thickness, density, and roughness of the films were obtained by fitting the XRR patterns using the Genx software [31]. Good fits to the XRR experimental patterns were obtained by considering two layers, including a diffusion layer and main layer. The diffusion of Co/Pd atoms into the substrate creates a very thin diffusion layer at the interface. The obtained data are summarized in Table I. The total thicknesses of the films were in the range of 15–18 nm. In order to study the role of film thickness on magnetic properties, especially in-plane anisotropy, a thicker film of $Co_{23}Pd_{77}$ with a thickness of 38 nm was also deposited on a MgO substrate. An increase of the Co:Pd ratio decreases the mass density of the films, as expected from the lower atomic mass of Co compared to Pd.

XRD patterns of the films are presented in Fig. 1. The films have an fcc-A_1 structure with preferred growth direction along [001]. The lattice parameter is calculated and summarized in Table I. It is seen that, because of the smaller atomic radius of Co relative to Pd, the lattice parameter of the film decreases with increasing the Co:Pd ratio. We note that an ordered $L1_0$ structure is only observed for FePd, FePt, and CoPt thin films, and is not formed in CoPd film, even for the equiatomic $Co_{50}Pd_{50}$ alloy [19].

B. Magnetic properties

Longitudinal MOKE hysteresis loops were measured as a function of the azimuthal angle between the applied magnetic field and the in-plane [100] direction of the MgO substrate. The measurements were performed by rotating the film around its normal axis and recording a loop every 10°. Both the coercivity and squareness of the hysteresis loops were extracted and are shown in Fig. 2 for Co_xPd_{100-x} ($x = 23, 36, 43$). Some of the hysteresis loops had a quadratic-MOKE (QMOKE) contribution (will be discussed below), which was systematically removed by symmetrization and antisymmetrization [32]. As can be seen in Fig. 2, the $Co_{23}Pd_{77}$ film shows fourfold in-plane anisotropy of the form

$$E(\theta) = 0.25K_4 \sin^2(2\theta), \tag{1}$$

where θ is the angle between the film magnetization and the [100] direction of the MgO substrate and K_4 is the fourfold cubic anisotropy constant. The easy axes of magnetization are along the [110] and [$\bar{1}$10] directions. Interestingly, by increasing the Co:Pd ratio, the symmetry of magnetic anisotropy changes to twofold in the $Co_{36}Pd_{64}$ and $Co_{43}Pd_{57}$ films. This modification is accompanied by a decrease of the coercivity. In this case the angular dependence of magnetic anisotropy energy can be written as

$$E(\theta) = K_U \sin^2(\theta), \tag{2}$$

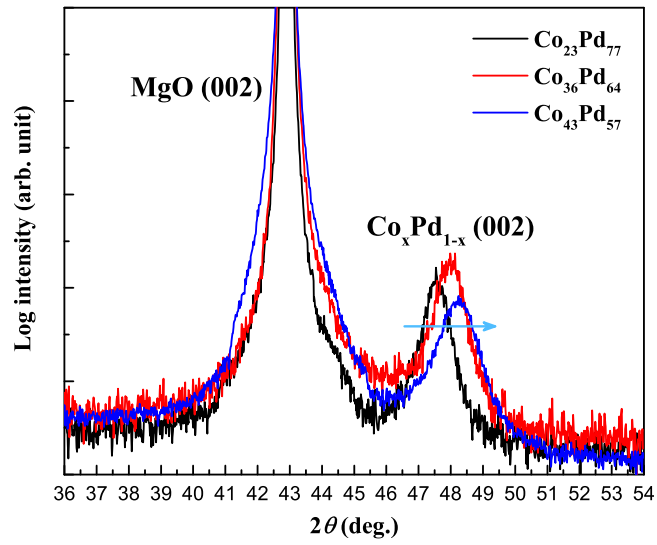

FIG. 1. XRD patterns of the CoPd thin films on MgO (001).

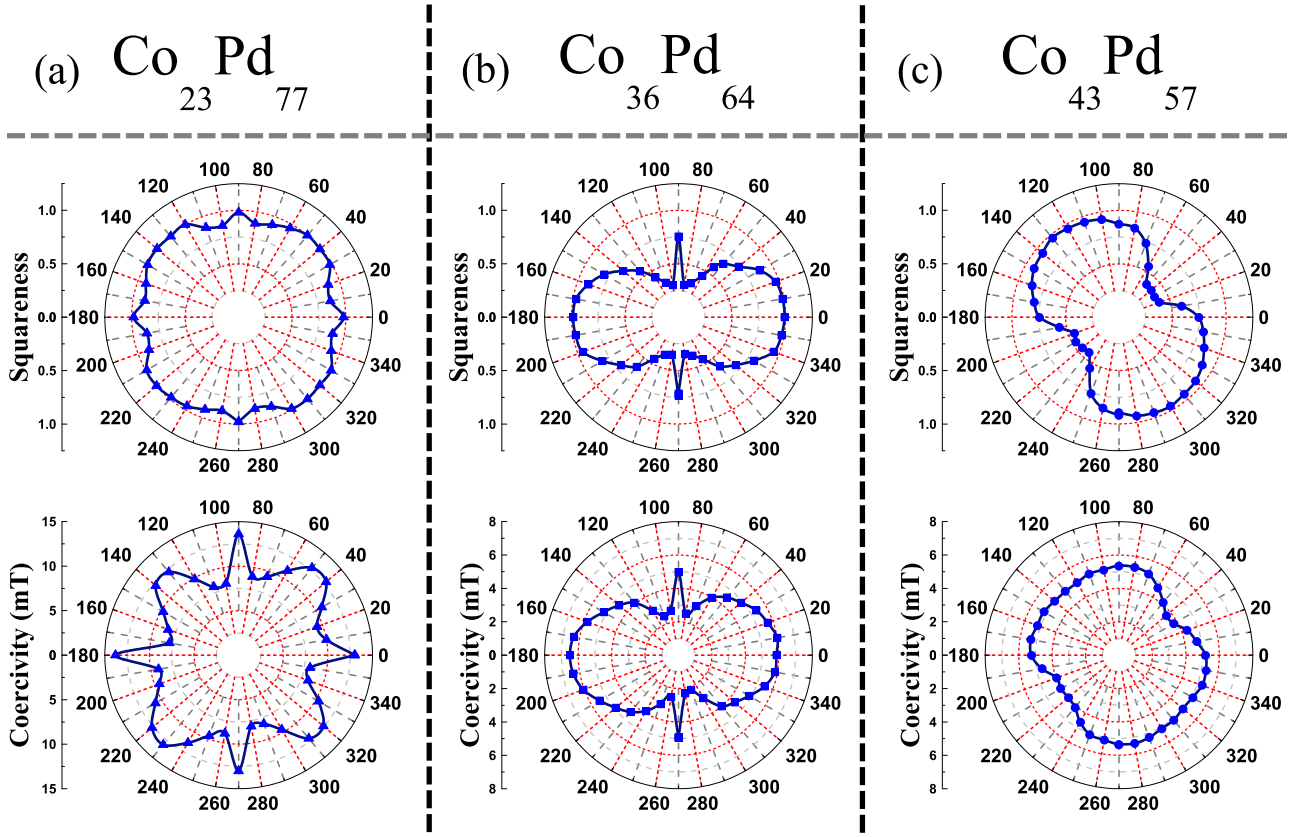

FIG. 2. Angular dependence of in-plane coercivity and hysteresis loop squareness for CoPd thin films with respect to the [100] direction of the MgO substrate. (a) $Co_{23}Pd_{77}$, (b) $Co_{36}Pd_{64}$, and (c) $Co_{43}Pd_{57}$.

where K_U is the uniaxial anisotropy constant. In the $Co_{36}Pd_{64}$ film, the easy magnetization axis is oriented along the [100] direction. However, in the $Co_{43}Pd_{57}$ film, the uniaxial anisotropy axis is rotated by 45° and oriented along $[\bar{1}10]$. Although the origin of this rotation is not fully clear, it is most likely induced by higher-order magnetoelastic contributions that arise from the smaller lattice parameter of the $Co_{43}Pd_{57}$ film rather than the $Co_{36}Pd_{64}$ film (see Table I). As the twofold anisotropy of the $Co_{36}Pd_{64}$ film is not changed in the $Co_{43}Pd_{57}$ film and coercivity of these two films are in the same order of magnitude (Fig. 2), it can be concluded that the rotation of easy axis is governed by magnetoelastic effects [33–35].

Spin-orbit coupling (SOC) is one of the key effects that can cause an enhancement of coercivity with decreasing Co:Pd ratio. In fact, an increase of the Pd content affects the magnetocrystalline anisotropy through SOC similar to Pt in $FePd_{1-x}Pt_x$ thin films [36]. Since the coercivity is related to the anisotropy constant as $H_C \propto K_4(K_U)/M_S$ a decrease of the cobalt content may also enhance the coercivity via a reduction of the saturation magnetization.

In the polar plots of Fig. 2, sharp peaks appear along the hard magnetization axes in the $Co_{23}Pd_{77}$ and $Co_{36}Pd_{64}$ films. This anomalous hard-axis magnetization reversal process disappears in the $Co_{43}Pd_{57}$ film. A collapse of hard-axis behavior has been observed also in other magnetic thin films, including Co thin films [37], Fe on Cu(001) [38], and $Co_2Cr_{0.6}Fe_{0.4}Al$ Heusler alloys on Cr/MgO(001) [39]. The origins of sharp peaks in the polar plots are mainly attributed to the existence of crystallographic disorder [40], frustration effects [39], or structural microdomains [38].

Idigoras *et al.* [40,41] presented a two-grain Stoner-Wohlfarth model to describe the magnetic behavior of thin films with misalignments between two weakly coupled grains. The in-plane anisotropy of our thin CoPd films is described correctly by this model. To illustrate this, we consider two misaligned grains with $\vec{m}_1$, $\vec{m}_2$ magnetization vectors and intergranular exchange coupling J [Fig. 3(a)]. For this system, the energy can be written as [40]

$$E = -J\vec{m}_1 \cdot \vec{m}_2 - \vec{H} \cdot (\vec{m}_1 + \vec{m}_2) - \tfrac{1}{2}K_1(\vec{m}_1 \cdot \vec{n}_1)^2 - \tfrac{1}{2}K_2(\vec{m}_2 \cdot \vec{n}_2)^2, \quad (3)$$

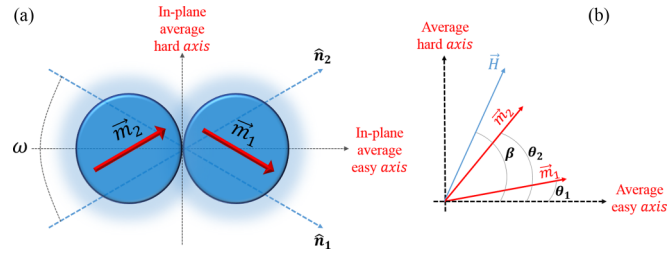

FIG. 3. Schematic of the two-grain Stoner-Wohlfarth model. (a) Illustration of magnetization vectors in two exchange-coupled grains and the orientation of their easy magnetization axes. (b) Angular definitions of the magnetic moments and the direction of magnetic field.

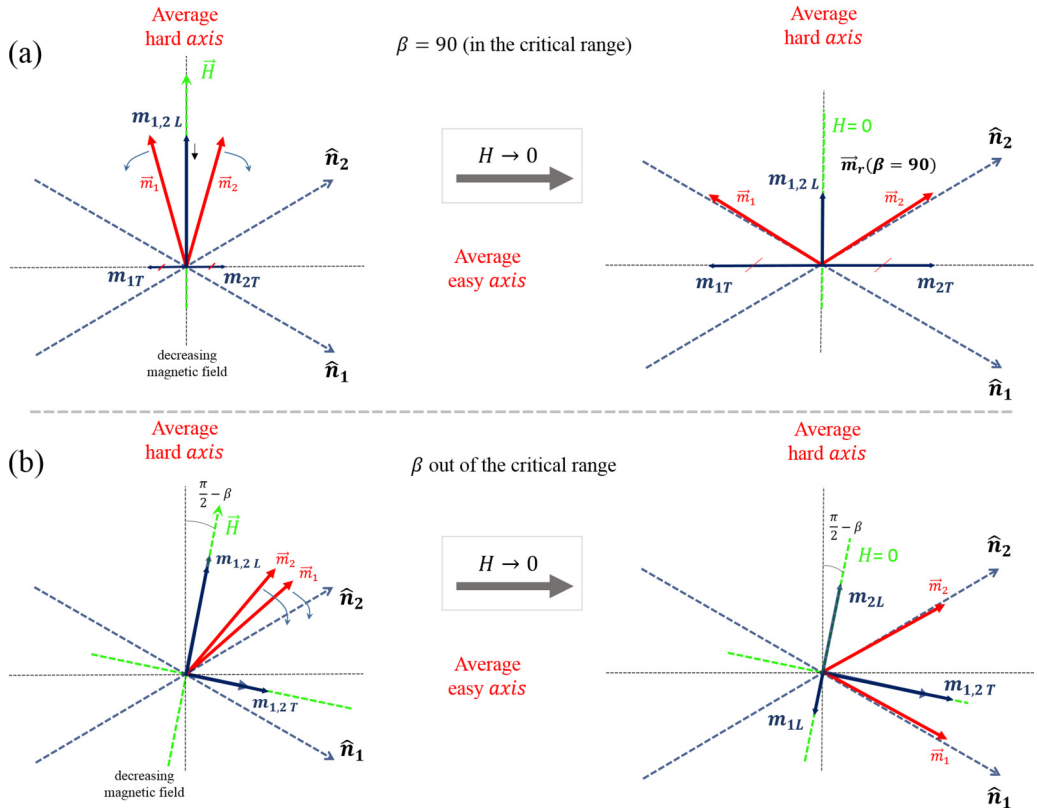

FIG. 4. (a) Formation of V-state mode by decreasing magnetic field and canceling out of the transverse magnetizations at $\beta = 90^\circ$ and (b) orientation of the magnetization vectors when β is out of the critical range and the appearance of a nonzero transverse magnetization.

where K_1 and K_2 are the magnetocrystalline anisotropy constants of the two grains and $\hat{n}_1$, $\hat{n}_2$ are their respective easy axes which are rotated by $+\omega/2$ and $-\omega/2$ from the average easy axis. If one assumes the magnetocrystalline anisotropy constants K_1 and K_2 to be identical because of good CoPd film homogeneity, the equation can be rewritten as [40]

$$E = -J\cos(\theta_1 - \theta_2) - H[\cos(\theta_1 - \beta) + \cos(\theta_2 - \beta)] - \tfrac{1}{2}K_1[\cos^2(\theta_1 + \omega/2) + \cos^2(\theta_2 - \omega/2)], \quad (4)$$

where θ_1 and θ_2 are the in-plane angles of $\vec{m}_1$ and $\vec{m}_2$ in the presence of a magnetic field. β indicates the direction of magnetic field, as shown in Fig. 3(b). According to the model, magnetization reversal depends on the magnetic field direction β, the ratio J/K_1, and the misalignment between the anisotropy axes of the two grains, ω.

To describe the sharp behavior in coercivity and remanent magnetization along hard axes, we depicted in Fig. 4 the orientations of $\vec{m}_1$ and $\vec{m}_2$ for two magnetic field orientations of $\beta = 90$ and $80\,(100)^\circ$. As discussed previously, there are two different easy axes that form an average easy axis. In order to minimize the energy, the angle between the magnetization moments can be ω or $\pi - \omega$ depending on the direction of the external magnetic field, β. For $\beta = 90^\circ$ (that magnetic field is perpendicular to the average easy axis), with reducing the field from saturation state to zero [Fig. 4(a)], because $\theta_1 + \omega/2$ is larger than 90°, $\vec{m}_1$ ($\vec{m}_2$) magnetization prefers to orient along $-\hat{n}_1$ ($+\hat{n}_2$). Thus, at $\mathrm{H}(\beta = 90^\circ) = 0$, a symmetric V-state forms between $\vec{m}_1$ and $\vec{m}_2$, which results in a relatively large net remanent magnetization ($M_L = m_{2L} + m_{1L}$), as depicted in the right side of Fig. 4(a). The anomalous sharp peaks are also seen in the coercivity (Fig. 2). This is because the magnetic field should bring out the magnetization moments from the stable states until the net magnetization becomes zero in the direction of applied field. One can predict that hard axes collapse occurs for $\beta = 90^\circ$ and angles which satisfy both $(\theta_1 + \omega/2) > 90$ and $(\theta_2 + \omega/2) < 90$. As shown in Fig. 4(b), for the magnetic field orientations close to the average hard axes (e.g., $\beta = 80$ or 100°), $\vec{m}_1$ and $\vec{m}_2$ would prefer to orient toward $+\hat{n}_1$ and $+\hat{n}_2$ directions or opposite, which results in a drop in the coercivity and the net remanent magnetization ($M_L = m_{2L} - m_{1L}$), as seen in Fig. 2.

Anomalous magnetization reversal in the two-grain Stoner-Wohlfarth model occurs when ω is considerably large or J/K_1 is small [40]. If we assume that ω is approximately the same for the $Co_{36}Pd_{64}$ and $Co_{43}Pd_{57}$ films, the disappearance of the sharp hard-axis features in the $Co_{43}Pd_{57}$ film [Fig. 2(c)] can be attributed to an increase of the J/K_1 ratio. This ratio is greater for $Co_{43}Pd_{57}$ because of higher Co content and lower anisotropy (resulted from Fig. 2). Therefore, with an increase of J/K_1, the V state does not form along the hard axis in the $Co_{43}Pd_{57}$ film. As the J/K_1 ratio increases, the intergranular exchange coupling energy [first term in Eq. (3)] outweighs the uniaxial anisotropy terms with different orientations. In this case, when $\vec{m}_2$ tends to orient along $+\hat{n}_2$, it also forces $\vec{m}_1$ to orient along $+\hat{n}_1$.

The above model is based on uniaxial anisotropy. However, the behavior of the $Co_{23}Pd_{77}$ film with fourfold in-plane magnetic anisotropy can be interpreted in a similar manner. For this case, easy and hard axes are shown in Fig. 5. It is

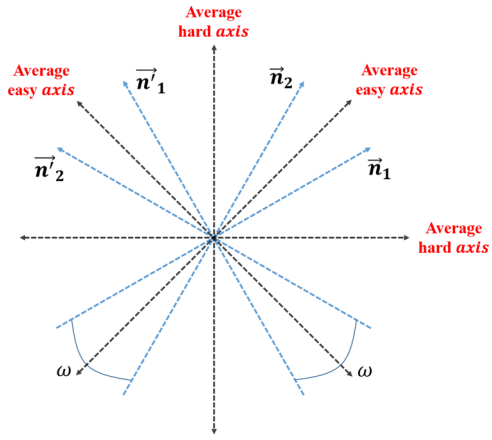

FIG. 5. Easy and hard average axes related to two grains with fourfold in-plane anisotropy.

reasonable to conclude that numbers of sharp peaks are equal to numbers of easy directions.

In order to understand the role of film thickness on the in-plane magnetic anisotropy, a thicker $Co_{23}Pd_{77}$ film is also deposited. In Fig. 6, polar curves of the films with two different thicknesses of 18.4 and 37.8 nm are shown. As can be seen, the fourfold anisotropy observed in $Co_{23}Pd_{77}$ does not depend on thickness, in the few tens of nanometers range. However, the thicker film has a smaller coercivity which may be due to a decrease of the magnetoelastic anisotropy. This is because induced stress depends on the lattice parameter of the film which is changed by both the Co:Pd ratio and thickness (see Table I). Magnetoelastic contributions mostly originate from the film-substrate lattice parameter misfit and have been reported to affect the magnetic characteristics and, in some cases, to totally alter the in-plane anisotropy [33,42,43].

To gain more insights into the anisotropy dispersion, FMR spectra of the films were measured by VNA-FMR technique. This technique allows exploring the in-plane anisotropy orientations of the films by measuring the resonance frequency

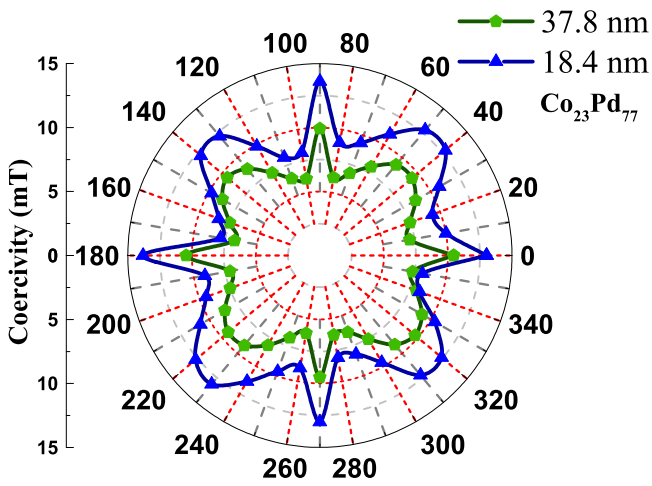

FIG. 6. Angular dependence of in-plane coercivity for the $Co_{23}Pd_{77}$ thin films on MgO substrates, with two different thicknesses of 18.4 and 37.8 nm.

within the range of 0–10 GHz. For this purpose, FMR spectra of the films were obtained at various in-plane orientations by changing the direction of the magnetic field relative to the MgO[100] direction. In the case of an in-plane applied magnetic field, the in-plane resonance frequency F is in the form of [44]

$$F = \frac{\gamma}{2\pi}(H_a H_b)^{1/2}, \tag{5}$$

where

$$\begin{aligned} H_a &= H\cos(\varphi_H - \varphi_M) + \frac{2K_4}{M_S}\cos 4(\varphi_M - \varphi_U) \\ &\quad + \frac{2K_U}{M_S}\cos(\varphi_M - \varphi_U), \\ H_b &= H\cos(\varphi_H - \varphi_M) + 4\pi M_{\text{eff}} \\ &\quad + \frac{K_4}{2M_S}[3 + \cos 4(\varphi_M - \varphi_U)] \\ &\quad + \frac{K_U}{M_S}[1 + \cos 2(\varphi_M - \varphi_U)], \end{aligned}$$

γ is the gyromagnetic factor, and φ_M (φ_H) is the in-plane angle between the magnetization (the applied magnetic field) and the MgO [100] direction. φ_U is the angle of one of the in-plane anisotropy easy axes with the MgO[100] direction. $M_{\text{eff}} = M_S - K_\perp/2\pi M_S$ is the effective magnetization where $K_\perp$ is the second-order out of plane uniaxial anisotropy constant. The angular dependence of the resonance frequency of the films is shown in Fig. 7. The dependence of the resonance frequency on the field orientation illustrates in-plane magnetic anisotropy. From Eq. (5), when $\varphi_M = \varphi_U$, F reaches its maximum and thus the extrema of the resonance frequency corresponds to the easy axes [44,45]. These results agree with the MOKE data (Fig. 2), except that the sharp hard-axis features are absent. This proves that the sharp peaks in the MOKE data do not correspond to conventional easy axes. Also, since the FMR polar plots, shown in Fig. 7, are not quite sinusoidal, they reflect the dispersed nature of the in-plane anisotropy of the films, as represented by different twofold and fourfold anisotropies in Figs. 4 and 5.

Here, it is necessary to discuss the role of the deposition process on the in-plane magnetic anisotropy of the CoPd thin films. In Fig. 8, the azimuthal dependence of coercivity for the $Co_{36}Pd_{64}$ film is compared with the same film deposited directly at 400 °C. Interestingly, the latter film shows an enhanced coercivity with no in-plane anisotropy. The SEM micrograph of the postannealed $Co_{36}Pd_{64}$ film, shown in Fig. 9(a), illustrates a mazelike pattern with a homogeneous grain size distribution. An island formation (Volmer-Weber) mode can be observed in the micrograph, as can be expected from the surface energies of metallic films on the oxide MgO substrate in an equilibrium regime [46–48]. On the other hand, the SEM micrograph of the $Co_{36}Pd_{64}$ film grown directly at 400 °C, shown in Fig. 9(b), exhibits a different microstructure (not island-growth mode) relative to the postannealed film. Thus the isotropic behavior of coercivity can be attributed to the random in-plane alignment of grains in the film. This reveals the crucial role of microstructure on the anisotropy characteristics [41,49]. Note that the XRD pattern of this film (not shown here) exhibited similar fcc-A_1 structure with a lattice constant of 3.81 Å.

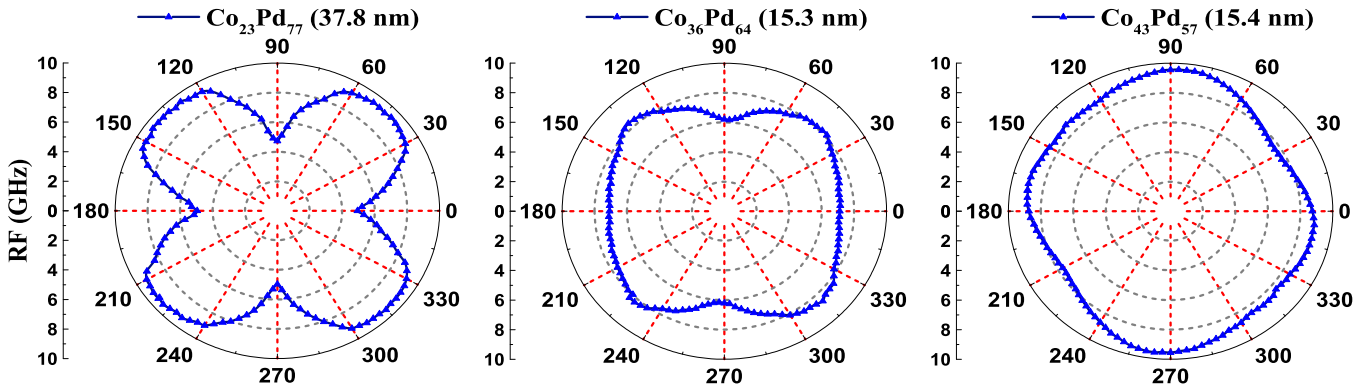

FIG. 7. Ferromagnetic resonance frequency (RF) as a function of azimuthal angle with respect to the in-plane [100] direction of MgO substrate. In the case of $Co_{23}Pd_{77}$ films, the RF data is presented for the thicker film (see Fig. 6). The FMR data was not detectable for the film with 18.4 nm thickness because of the small magnetic signal.

C. QMOKE and its relation with the two-grain Stoner-Wohlfarth model

To further confirm the above model, it is useful to investigate the appearance of QMOKE in the hysteresis loops. This is because QMOKE is sensitive to transverse magnetization. As shown in Fig. 10, because of QMOKE contribution, MOKE measurements show some irregular magnetic hysteresis loops at azimuthal angles near the nominal hard axes, but not exactly along them. This irregular behavior gradually disappears if the field angle rotates to the average easy axis. Furthermore, in our results, the QMOKE contribution decreases if the magnetic anisotropy is lowered through an increase of the Co:Pd ratio.

The optical and magneto-optical properties of materials can be described by a permittivity tensor ε_{ij}, which can be expanded into a power series of Cartesian direction cosines M_i of magnetization [50,51]:

$$\varepsilon_{ij} = \varepsilon_{ij}^{(0)} + K_{ijk}M_k + G_{ijkl}M_kM_l + \cdots, \tag{6}$$

where M_i are the components of the magnetization. K_{ijk} and G_{ijkl} are the linear and quadratic magneto-optical tensors, respectively. $\varepsilon_{ij}^{(0)}$ is the permittivity tensor in the absence of magnetic ordering. For cubic crystal structures (such as A_1 structure), the number of independent tensor elements reduces to five parameters including one free (complex) parameter in the constant term $\varepsilon_{ij}^{(0)}$, another one (K) in the linear term K_{ijk}, and three additional parameters called G_{11}, G_{12}, and G_{44} in the quadratic term G_{ijkl}. As a result, for a magnetized film with cubic symmetry and in-plane magnetization, complex Kerr amplitude ϕ is defined as [50]

$$\phi_{s/p} = \mp B_{s/p} K M_L \pm A_{s/p}\left[2G_{44} + \frac{\Delta G}{2}(1-\cos 4\beta)\right] \times M_L M_T \mp A_{s/p}\frac{\Delta G}{4}\sin 4\beta\left(M_L^2 - M_T^2\right), \tag{7}$$

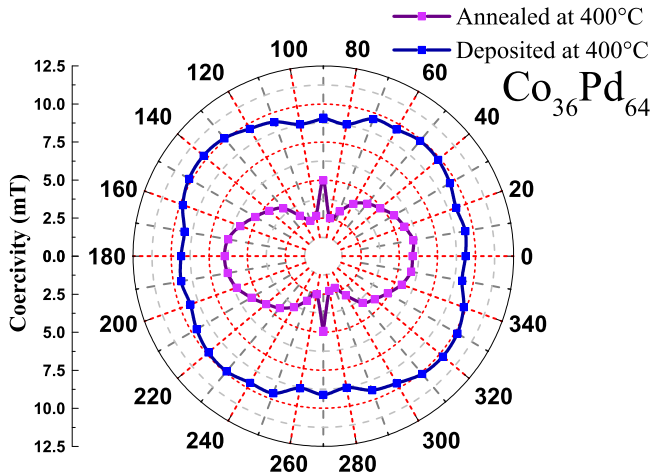

FIG. 8. In-plane magnetic anisotropy of the $Co_{36}Pd_{64}$ thin films, RT deposited, followed by annealing at 400 °C and directly deposited at 400 °C.

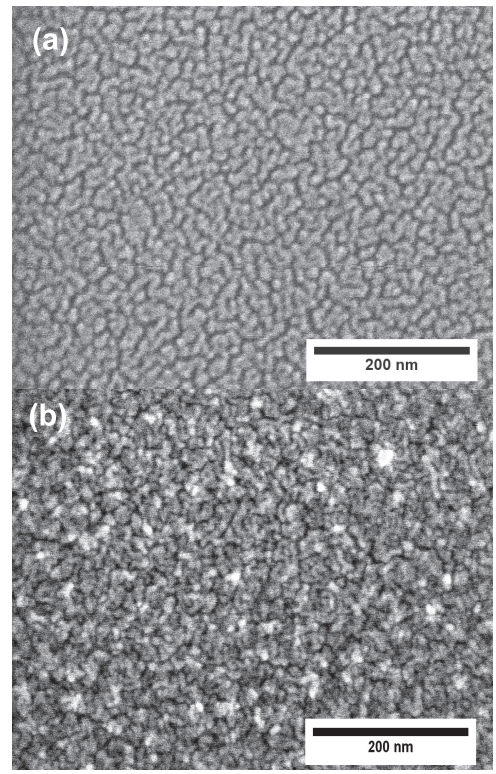

FIG. 9. SEM micrographs of the $Co_{36}Pd_{64}$ films (a) RT deposited, followed by annealing at 400 °C, and (b) directly deposited at 400 °C.

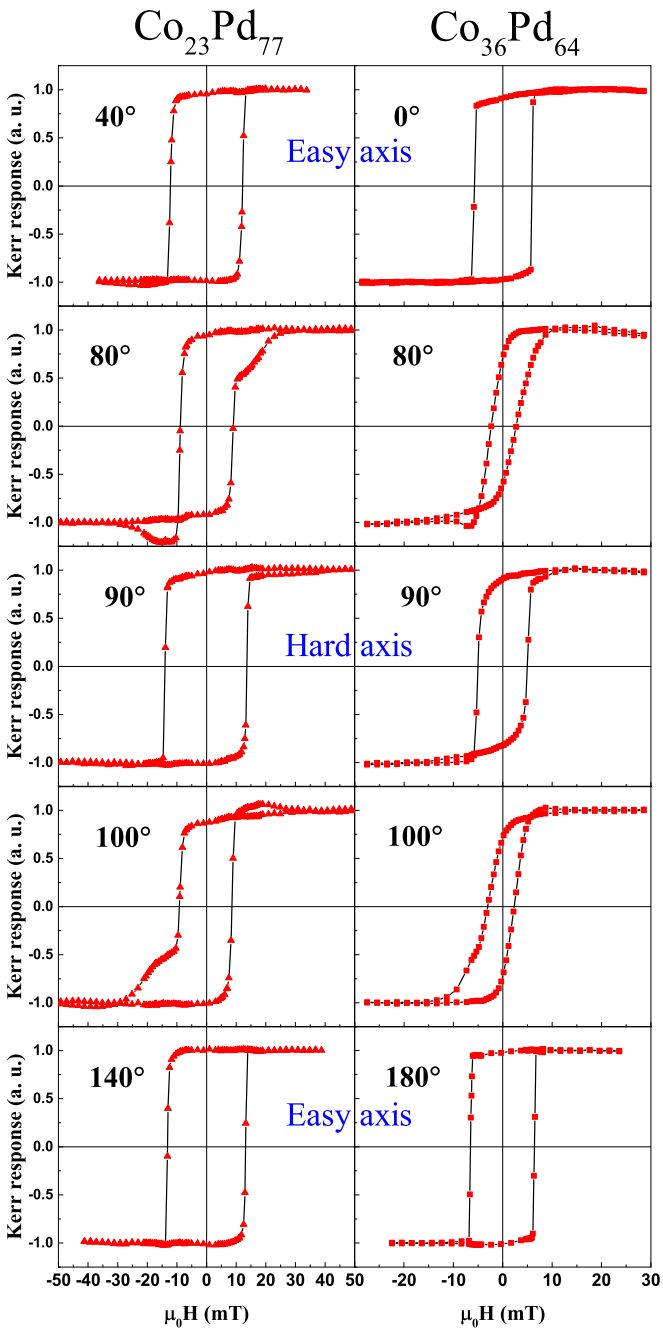

FIG. 10. MOKE hysteresis loops of $Co_{23}Pd_{77}$ and $Co_{36}Pd_{64}$ thin films at angles close to the easy and hard magnetization axes.

where $-(+)$ is related to $s(p)$ incident polarized light, $A_{s/p}$ and $B_{s/p}$ are functions of the angle of incident, M_L and M_T are longitudinal and transversal components of magnetization, $\Delta G = G_{11} - G_{12} - 2G_{44}$ is the so-called magneto-optic anisotropy parameter, and β specifies sample orientation. The linear Kerr response [first term in Eq. (7)] is used normally to obtain magneto-optical hysteresis loops. However, quadratic contributions [next terms in Eq. (7)] in L-MOKE measurements tend to an irregular hysteresis loop, which is mainly due to the presence of transverse magnetization M_T. In the Stoner-Wohlfarth model, QMOKE is expected to appear at hard axes. However, as mentioned above, in our results QMOKE is not observed at the hard axes (90° loops in Fig. 10) of $Co_{23}Pd_{77}$ and $Co_{36}Pd_{64}$ films. This behavior originates from anisotropy dispersion and can be explained using the two-grain Stoner-Wohlfarth model. As shown in Fig. 4(a), when the magnetic field reduces from saturation state, the magnetization moments $\vec{m}_1$ and $\vec{m}_2$ rotate counterclockwise and clockwise, respectively, and thus the net transverse magnetization becomes zero ($M_T = m_{1T} - m_{2T} = 0$), which leads to the vanishing of QMOKE based on Eq. (7). On the other hand, for field directions near the nominal hard axes (80° or 100° loops in Fig. 10), the symmetric V state does not form [shown in Fig. 4(b)] and a nonzero net transverse magnetization is expected to produce a QMOKE signal in hysteresis measurements. In fact, our QMOKE data reveals the validity of the two-grain Stoner-Wohlfarth model.

IV. SUMMARY

Structural and magnetic properties of Co_xPd_{100-x} ($x = 23, 36, 43$) thin films (15–18 nm) on MgO are investigated in order to study the effect of intergranular exchange interaction on the magnetization reversal process in weakly disordered films. CoPd/MgO can exhibit fourfold or twofold in-plane magnetic anisotropy depending on the Co:Pd ratio. For lower cobalt contents ($x = 23, 36$), anomalous magnetization reversal occurs when the magnetic field is oriented along the nominal hard axes. However, this so-called anomalous hard axis collapse does not occur in films with $x = 43$ because the larger cobalt content enhances the intergranular exchange interaction. The dependence of anisotropy on Co:Pd ratio is also confirmed by ferromagnetic resonance (FMR) measurements. However, since anomalous behavior is absent in the FMR data, we conclude that the hard-axis peaks are not caused by conventional easy-axis behavior. Our results are explained within the framework of the two-grain Stoner-Wohlfarth model, as confirmed by the occurrence of a quadratic magneto-optical Kerr effect.

In order to further investigate the anisotropy behavior, the effect of film thickness and growth conditions are also discussed. The $Co_{23}Pd_{77}$ film shows a similar fourfold in-plane anisotropy but a reduced coercivity when its film thickness is increased to 38 nm. We also investigated the role of film microstructure on the anisotropy characteristics by employing two different protocols for the preparation of films: the first consisted of film deposition at room temperature followed by short time postannealing at 400 °C and the second involved direct deposition of the films at 400 °C. The results show that the in-plane magnetic anisotropy is established during the annealing step.

ACKNOWLEDGMENTS

This work was supported by Isfahan University of Technology (IUT). We acknowledge the provision of facilities and technical support by Aalto University at OtaNano–Nanomicroscopy Center (Aalto-NMC).

[1] D. Navas, N. Soriano, F. Béron, C. T. Sousa, K. R. Pirota, J. Torrejon, C. Redondo, R. Morales, and C. A. Ross, Phys. Rev. B **96**, 180403 (2017).

[2] B. J. Kirby, J. E. Davies, K. Liu, S. M. Watson, G. T. Zimanyi, R. D. Shull, P. A. Kienzle, and J. A. Borchers, Phys. Rev. B **81**, 100405 (2010).

[3] A. K. Nayak, M. Nicklas, S. Chadov, P. Khuntia, C. Shekhar, A. Kalache, M. Baenitz, Y. Skourski, V. K. Guduru, A. Puri *et al.*, Nat. Mater. **14**, 679 (2015).

[4] K. Yoshii, Appl. Phys. Lett. **99**, 142501 (2011).

[5] B. Li, R. V. Chopdekar, E. Arenholz, A. Mehta, and Y. Takamura, Appl. Phys. Lett. **105**, 202401 (2014).

[6] Y. Liu, S. G. E. te Velthuis, J. S. Jiang, Y. Choi, S. D. Bader, A. A. Parizzi, H. Ambaye, and V. Lauter, Phys. Rev. B **83**, 174418 (2011).

[7] J.-L. Tsai, H.-T. Tzeng, and G.-B. Lin, Appl. Phys. Lett. **96**, 032505 (2010).

[8] T. M. d. L. Alves, C. G. Bezerra, A. Viegas, S. Nicolodi, M. A. Corrêa, and F. Bohn, J. Appl. Phys. **117**, 083901 (2015).

[9] C. Hamann, J. McCord, L. Schultz, B. P. Toperverg, K. Theis-Bröhl, M. Wolff, R. Kaltofen, and I. Mönch, Phys. Rev. B **81**, 024420 (2010).

[10] X. Liu and G. Zangari, J. Appl. Phys. **90**, 5247 (2001).

[11] E. Torok, J. Appl. Phys. **36**, 952 (1965).

[12] X. Wu, H. Zhou, R. van de Veerdonk, T. Klemmer, and D. Weller, J. Magn. Magn. Mater. **278**, 285 (2004).

[13] N. Sun and S. Wang, J. Appl. Phys. **93**, 6468 (2003).

[14] B. Dieny and M. Chshiev, Rev. Mod. Phys. **89**, 025008 (2017).

[15] R. H. Liu, W. L. Lim, and S. Urazhdin, Phys. Rev. Lett. **114**, 137201 (2015).

[16] D. Erdem, N. S. Bingham, F. J. Heiligtag, N. Pilet, P. Warnicke, L. J. Heyderman, and M. Niederberger, Adv. Funct. Mater. **26**, 1954 (2016).

[17] E. Sallica Leva, R. C. Valente, F. Martinez Tabares, M. Vasquez Mansilla, S. Roshdestwensky, and A. Butera, Phys. Rev. B **82**, 144410 (2010).

[18] M. Mulazzi, A. Chainani, Y. Takata, Y. Tanaka, Y. Nishino, K. Tamasaku, T. Ishikawa, T. Takeuchi, Y. Ishida, Y. Senba *et al.*, Phys. Rev. B **77**, 224425 (2008).

[19] M. Ohtake, S. Ouchi, F. Kirino, and M. Futamoto, J. Appl. Phys. **111**, 07A708 (2012).

[20] J. M. Coey, *Magnetism and Magnetic Materials* (Cambridge University Press, Cambridge, UK, 2010).

[21] L. Vivas, J. Rubin, A. Figueroa, F. Bartolomé, L. Garcia, C. Deranlot, F. Petroff, L. Ruiz, J. Gonzalez-Calbet, S. Pascarelli *et al.*, Phys. Rev. B **93**, 174410 (2016).

[22] S. D. Pollard, J. A. Garlow, J. Yu, Z. Wang, Y. Zhu, and H. Yang, Nat. Commun. **8**, 14761 (2017).

[23] B. Clark, A. Natarajarathinam, Z. Tadisina, P. Chen, R. Shull, and S. Gupta, J. Magn. Magn. Mater. **436**, 113 (2017).

[24] P.-C. Chang, Y.-C. Chen, C.-C. Hsu, V. R. Mudinepalli, H.-C. Chiu, and W.-C. Lin, J. Alloys Compd. **710**, 37 (2017).

[25] V. R. Mudinepalli, Y.-C. Chen, P.-C. Chang, C.-C. Hsu, C.-Y. Tsai, H.-C. Chiu, C.-T. Wu, H.-W. Yen, S.-J. Shih, and W.-C. Lin, J. Alloys Compd. **695**, 2365 (2017).

[26] W.-C. Lin, C.-J. Tsai, B.-Y. Wang, C.-H. Kao, and W.-F. Pong, Appl. Phys. Lett. **102**, 252404 (2013).

[27] W.-C. Lin, C.-J. Tsai, H.-Y. Huang, B.-Y. Wang, V. R. Mudinepalli, and H.-C. Chiu, Appl. Phys. Lett. **106**, 012404 (2015).

[28] M. Zhernenkov, M. R. Fitzsimmons, J. Chlistunoff, J. Majewski, I. Tudosa, and E. E. Fullerton, Phys. Rev. B **82**, 024420 (2010).

[29] J.-H. Kim, K.-S. Ryu, J.-W. Jeong, and S.-C. Shin, Appl. Phys. Lett. **97**, 252508 (2010).

[30] E. Gan'shina, V. Guschin, I. Romanov, A. Skobelev, and A. Tselev, J. Magn. Magn. Mater. **193**, 174 (1999).

[31] M. Björck and G. Andersson, J. Appl. Crystallogr. **40**, 1174 (2007).

[32] O. Gaier, J. Hamrle, S. Hermsdoerfer, H. Schultheiß, B. Hillebrands, Y. Sakuraba, M. Oogane, and Y. Ando, J. Appl. Phys. **103**, 103910 (2008).

[33] O. Thomas, Q. Shen, P. Schieffer, N. Tournerie, and B. Lépine, Phys. Rev. Lett. **90**, 017205 (2003).

[34] Y.-S. Zhang, W. He, J. Tang, S. S. Ahmad, W. Zhang, Y. Li, X.-Q. Zhang, and Z.-H. Cheng, AIP Adv. **7**, 056326 (2017).

[35] Y. Shirahata, T. Nozaki, G. Venkataiah, H. Taniguchi, M. Itoh, and T. Taniyama, Appl. Phys. Lett. **99**, 022501 (2011).

[36] X. Ma, P. He, L. Ma, G. Guo, H. Zhao, S. Zhou, and G. Lüpke, Appl. Phys. Lett. **104**, 192402 (2014).

[37] K. Zhang, R. Gupta, K. Lieb, Y. Luo, G. Müller, P. Schaaf, and M. Uhrmacher, Europhys. Lett. **64**, 668 (2003).

[38] F. Scheurer, R. Allenspach, P. Xhonneux, and E. Courtens, Phys. Rev. B **48**, 9890 (1993).

[39] J. Hamrle, S. Blomeier, O. Gaier, B. Hillebrands, R. Schäfer, and M. Jourdan, J. Appl. Phys. **100**, 103904 (2006).

[40] O. Idigoras, A. K. Suszka, P. Vavassori, P. Landeros, J. M. Porro, and A. Berger, Phys. Rev. B **84**, 132403 (2011).

[41] O. Idigoras, A. Suszka, P. Vavassori, B. Obry, B. Hillebrands, P. Landeros, and A. Berger, J. Appl. Phys. **115**, 083912 (2014).

[42] W. Liao, S. Chen, F. Yuan, C. Hsu, and H. Lee, J. Magn. Magn. Mater. **303**, e243 (2006).

[43] J. Gong, S. Riemer, M. Kautzky, and I. Tabakovic, J. Magn. Magn. Mater. **398**, 64 (2016).

[44] M. Belmeguenai, F. Zighem, Y. Roussigné, S. M. Chérif, P. Moch, K. Westerholt, G. Woltersdorf, and G. Bayreuther, Phys. Rev. B **79**, 024419 (2009).

[45] O. Acher, S. Queste, M. Ledieu, K.-U. Barholz, and R. Mattheis, Phys. Rev. B **68**, 184414 (2003).

[46] L. Martin, Y.-H. Chu, and R. Ramesh, Mater. Sci. Eng., R **68**, 89 (2010).

[47] M. Rahman and J.-K. Park, J. Appl. Phys. **120**, 165302 (2016).

[48] T. Suzuki, K. Harada, N. Honda, and K. Ouchi, J. Magn. Magn. Mater. **193**, 85 (1999).

[49] S. Trudel, G. Wolf, J. Hamrle, B. Hillebrands, P. Klaer, M. Kallmayer, H.-J. Elmers, H. Sukegawa, W. Wang, and K. Inomata, Phys. Rev. B **83**, 104412 (2011).

[50] K. Postava, D. Hrabovskỳ, J. Pištora, A. Fert, Š. Višňovskỳ, and T. Yamaguchi, J. Appl. Phys. **91**, 7293 (2002).

[51] M. Buchmeier, R. Schreiber, D. E. Bürgler, and C. M. Schneider, Phys. Rev. B **79**, 064402 (2009).